Weight Minimization of In-Plane Structures Using Implicit Floating Projection Topology Optimization

Settawuth Rattanaudom[1] Sawekchai Tangaramvong[2,*] and Rut Su[3]

[1,2,3] *Department of Civil Engineering, Faculty of Engineering, Chulalongkorn University, Bangkok, THAILAND*
**Corresponding author; E-mail address: sawekchai.t@chula.ac.th*

Abstract

This research introduces an innovative approach to minimizing the weight of in-plane structures using the implicit three-field Floating Projection Topology Optimization (FPTO) method. The FPTO method employs numerical simulation to enforce 0/1 design variable constraints, enabling the generation of clearly optimized designs with fewer intermediate elements. A key feature of this study is the adaptation of the original compliance minimization algorithm within the FPTO method, focusing on weight reduction driven by the maximum compliance ratio. Benchmark case studies validate the effectiveness of the proposed method, demonstrating weight reductions compared to existing techniques. Specifically, the method achieves a 10% weight saving in a two-bar truss. This result highlights the potential of using the FPTO method as an optimization tool for designing lightweight in-plane structures while maintaining structural performance.

Keywords: Topology Optimization, Weight Minimization, Floating Projection Topology Optimization, Maximum Compliance Ratio

1. Introduction

Topology Optimization (TO) is a numerical method for obtaining the optimal material distribution within a specified design domain under loading and boundary conditions [1]. The optimization process aims to minimize an objective function, which is often structural compliance, where a lower compliance corresponds to a lower total strain energy. TO has become a powerful tool for designing optimal structural configurations by determining the arrangement of material and the connectivity of elements. This numerical method is widely applied in various engineering fields, including structural engineering, aerospace, automotive, and biomedical engineering. For instance, [2] demonstrated the effectiveness of TO in minimizing the weight of aircraft components while maintaining structural integrity under maximum stress constraints. Similarly, [3] applied TO in designing the internal structure of artificial bone implants, ensuring biomechanical compatibility with patient-specific anatomical features. These examples demonstrate the versatility of TO in addressing complex engineering problems, provided the design domain, loading conditions, and boundary constraints are well-defined.

Over the past few decades, TO has undergone significant advancements, evolving into multiple methodological variations. A significant breakthrough in TO development was the introduction of the 99-line topology optimization MATLAB code by [4], which significantly simplified TO implementations, and facilitated further research. According to [5], TO methodologies can be broadly classified into three main approaches: (1) density-based methods, (2) differential equation-driven approaches, commonly referred to as the level-set method, and (3) geometric component-based methods. This study primarily concentrates on density-based methods, where the optimization is performed at the level of individual elements or nodes within the structure.

The density-based approach can be further divided into two subcategories: the Solid Isotropic Material with Penalization (SIMP) method [6] and discrete variable approaches. The SIMP method defines each element's density as a continuous variable ranging between 0 (void) and 1 (solid), with intermediate values influencing material properties through an interpolation scheme. To achieve the design of a clear 0/1 structure, a penalization technique is employed, pushing the intermediate densities closer to 0/1 values. However, the presence of intermediate elements in the transition zones between solid and void regions remains a challenge. Alternatively, discrete variable approaches assign binary values (0 or 1) to each element, ensuring a purely discrete topology. While this method eliminates the need for penalization, directly enforcing many binary constraints results in excessive computational costs, making its practical implementation challenging. Consequently, heuristic-based methods, such as Evolutionary Structural Optimization (ESO) [7] and Bi-directional Evolutionary Structural Optimization (BESO) [8-10], have been developed to address these limitations by gradually removing and adding elements during the optimization process. Despite their advantages, these evolutionary-based approaches are often plagued by instability and convergence issues.

To overcome the challenges associated with SIMP and evolutionary-based approaches, [11, 12] introduced the Floating Projection Topology Optimization (FPTO) method. FPTO integrates the implicit Floating Projection (FP) constraint, which effectively simulates the enforcement of 0/1 constraints without relying on explicit penalization or material interpolation functions. This method has been shown to significantly reduce the occurrence of intermediate densities, offering greater stability compared to evolutionary-based approaches. FPTO has been successfully applied in various structural optimization problems, including multi-material topology optimization [13, 14], mechanical-acoustic interaction structures [15], and chiral metamaterial structures [16]. The core principle of FPTO involves progressively tightening the range of permissible design variable values over inner optimization loops while leveraging the optimality criterion (OC) method [17] for efficient updates.

In addition to the classical compliance minimization, no one has explored the integration of FPTO with quadtree adaptive meshing techniques for structural weight minimization. This research aims to bridge that gap by combining the FPTO algorithm with quadtree-based adaptive meshing and utilizing the SBFE framework to perform structural analysis. The proposed methodology is validated by comparing the weight minimization results against benchmark problems [18]. By leveraging this novel integration, the study enhances computational efficiency while achieving high-quality 0/1 topology designs, thereby advancing the field of TO for complex structural systems.

2. Problem Formulations

2.1 Weight Minimization Topology Optimization

This research aims to minimize the weight of a continuum structure, subject to a structural compliance constraint, using the finite element analysis framework and can be numerically expressed as:

$$\text{Minimize}: \quad W = \sum_{\mathrm{N}} x_{\mathrm{e}} V_{\mathrm{e}} \tag{1}$$

$$\text{Subject to}: \quad \mathbf{K}(x)\mathbf{U} = \mathbf{F} \tag{2}$$

$$C / \left(\alpha_{\mathrm{C}} C_0\right) \leq 1 \tag{3}$$

$$C = \mathbf{F}^T \mathbf{U} \tag{4}$$

$$x_{\min} \leq x_{\mathrm{e}} \leq 1 \tag{5}$$

where W is the structural weight, x_e is the element density, V_e is the element volume, which is a constant value since all elements are the same size in uniform meshing scheme. Equation (2) enforces the structural equilibrium, where K is global stiffness matrix, U is displacement vector, and F is force vector. Equation (3) enforces the maximum compliance constraint, where C is the structural compliance, α_c is the maximum compliance ratio, and C_0 is the evaluated structural compliance on the full domain design. By enforcing maximum compliance constraint, the structural compliance in each iteration is forced to be lower than the maximum compliance ratio times structural compliance of the full domain design. x_e is the design variables or elemental density, where 0 and 1 represent void and solid element respectively.

The optimization process starts with relaxation on design variables and can be expressed as: $0 < x_{min} \leq x_e \leq 1$, where x_{min} is recommended to be a small positive number, such as 10^{-6}. Then, the linear material interpolation scheme is employed to adjust the material properties based on each element density and can be expressed as:

$$\mathbf{D}(x_e) = x_e \mathbf{D}^1 \tag{6}$$

The problems are defined as a linear elastic isotropic solid material in a two-dimensional plane-stress, with no body force. The constitutive matrix for each element can be expressed as:

$$\mathbf{D}^1 = \frac{E}{1-\nu^2}\begin{pmatrix} 1 & \nu & 0 \\ \nu & 1 & 0 \\ 0 & 0 & \frac{1-\nu}{2} \end{pmatrix} \tag{7}$$

$$V(x_e) = x_e V_e \tag{8}$$

where E is the elastic modulus, and ν is Poisson's ratio, which is equal to 0.30. Therefore, the structural compliance and the volume fraction can be rewritten as:

$$C = \sum_e x_e \mathbf{u}_e^T \mathbf{k}^1 \mathbf{u}_e \tag{9}$$

$$\mathbf{k}^1 = \int_{V^e} \mathbf{B}^T \mathbf{D}^1 \mathbf{B} dV \tag{10}$$

$$V_f = \frac{\sum_e x_e V_e}{\sum_e V_e} \tag{11}$$

where u_e is the displacement vector for each element, k^1 is the stiffness matrix of solid element, B is the strain-displacement matrix, and V_f is the volume fraction of the structure. For the TO process, the sensitivity of the compliance and volume fraction is calculated as:

$$\frac{\partial C}{\partial x_e} = -\mathbf{u}^T \frac{\partial \mathbf{K}}{\partial x_e}\mathbf{u} = -\mathbf{u}_e^T \mathbf{k}^1 \mathbf{u}_e \tag{12}$$

$$\frac{\partial V_f}{\partial x_e} = \frac{V_e}{\sum_e V_e} \tag{13}$$

2.2 Modified Implicit Three-Field FPTO Topology Optimization

The originally proposed three-field TO by [11, 12] separates the design variables into three fields: the design field ($\bar{x}_e$), the filter field ($\tilde{x}_e$), and the physical (projection) field (x_e). In the three-field TO, the process aims to find the optimal design in the design field before projecting it to the physical field as the optimal solution. The optimization process can be summarized in the following flowchart.

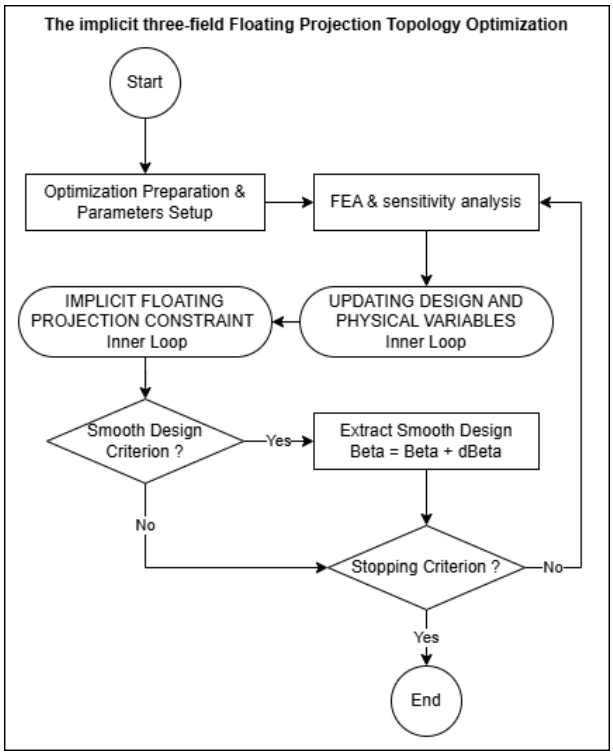

Fig. 1 Flowchart of the implicit three-field Floating Projection Topology Optimization.

At the start of the optimization process, the initial solution in the design field is processed through finite element analysis and then enters the first inner loop called "UPDATING DESIGN AND PHYSICAL VARIABLES", where the design variables in the design field are filtered into the filter field using the following expression:

$$x_e = \sum_j w_{ej} \bar{x}_j \tag{14}$$

$$w_{ej} = \frac{r_{\min} - r_{ej}}{\sum_j (r_{\min} - r_{ej})} \quad \text{for} \quad j \in N_c \tag{15}$$

$$w_{ej} = 0 \quad \text{for} \quad j \notin N_c \tag{16}$$

where w_{ej} is the weight factor for each element in the design field $\bar{x}_j$. r_{ej} is the distance between element e and element j. r_{min} is a filtering radius centered at element e, and N_c is a circular domain centered at element e with radius of r_{min}. After the filtering process, the design variables in the filter field ($\tilde{x}_e$) are transformed into the physical field (x_e) using the Heaviside projection, which can be expressed as:

$$x_e = \frac{\tanh(\beta_1 \cdot \eta) + \tanh(\beta_1 \cdot (x_e - \eta))}{\tanh(\beta_1 \cdot \eta) + \tanh(\beta_1 \cdot (1 - \eta))} \tag{17}$$

where $\beta_1 = 1.2\beta$

β_1 is the steepness of the Heaviside projection function, and η is the constant to define whether an eroded design or dilated design is desirable. For typical designs, η = 0.5. Therefore, the sensitivity of the compliance and volume fraction can be rewritten as the differential of the design variables in the design field ($\bar{x}_e$) as:

$$\frac{\partial C}{\partial \bar{x}_e} = \frac{\partial C}{\partial x_e} \frac{\partial x_e}{\partial x_e} \frac{\partial x_e}{\partial \bar{x}_e} \tag{18}$$

$$\frac{\partial V_f}{\partial \bar{x}_e} = \frac{\partial V_f}{\partial x_e} \frac{\partial x_e}{\partial x_e} \frac{\partial x_e}{\partial \bar{x}_e} \tag{19}$$

The Optimality Criterion (OC) optimizer is employed to update the design variables in the design field with the sensitivity of the compliance and volume fraction. The equation is as follows:

$$\bar{x}_e = (\bar{x}_e)_{k-1} \left(-\lambda \cdot \frac{\partial C}{\partial \bar{x}_e} \Big/ \frac{\partial V_f}{\partial \bar{x}_e} \right)^{\frac{1}{2}} \tag{20}$$

where $(\bar{x}_e)_{k-1}$ is the design variables in the design field of previous iteration, and λ is the Lagrange multiplier, which is determined by bisection inner loop called "updating design and physical variables".

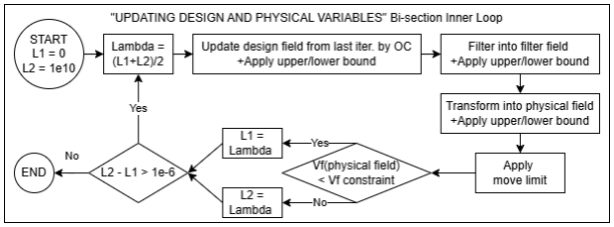

Fig. 2 Flowchart of the bisection of the inner loop for updating design and physical variables.

As shown in Fig. 2, the bisection inner loop will iterate until the bisection's tolerance is satisfied, leading to the potential way to modify and let the inner loop iterate until the compliance constraint in equation (3) are satisfied. The modification is done by changing the satisfaction criteria from $V_f(x_e) < \bar{V}_f$ to $C(x_e)/C_0 > \alpha_c$. The difference between the sign ">" and "<" is caused by the inverse relationship between volume and compliance. From the experimental numerical simulation, the optimality criterion in equation (20) should be modified to:

$$\bar{x}_e = (\bar{x}_e)_{k-1}\left(-\lambda \cdot \frac{\partial C}{\partial \bar{x}_e}\right)^{\frac{1}{2}} \quad (21)$$

Additionally, the structural compliance should be calculated within the bisection inner loop. The modified bisection inner loop is shown in Fig. 3.

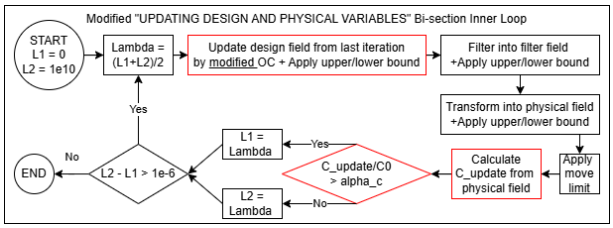

Fig. 3 Flowchart of the modified bisection inner loop for updating design and physical variables.

When the compliance constraint is satisfied, the optimal design in each field is achieved. Note that in the bisection inner loop, the upper bound (=1) and lower bound (x_{min} = 10^{-6}) are employed in every transformation to another field. The move limit (δ = 0.2) is also employed during the transformation into the physical field, enforcing that the value of element e in the physical field (x_e) remains within the range [x_e^{k-1}-δ, x_e^{k-1}+δ], where x_e^{k-1} is element e in the physical field from the previous iteration.

From the first bisection inner loop, the optimal design in the design field ($\bar{x}_e$) might not be sufficiently clear since the design variables have been relaxed at the start of the TO process. Therefore, the implicit filtering and FP constraints must be employed to numerically simulate 0/1 constraints on the design variables. The expression of implicit filtering is the same as equation (14), and the implicit FP constraint is expressed as:

$$(\bar{x}_e)_k = \frac{\tanh(\beta \cdot th) + \tanh(\beta \cdot (x_e - th))}{\tanh(\beta \cdot th) + \tanh(\beta \cdot (1 - th))} \quad (22)$$

where $(\bar{x}_e)_k$ is the design variables in the design field at the current iteration, and th is the floating threshold that is determined by second bisection inner loop called "IMPLICIT FLOATING PROJECTION (FP) CONSTRAINT FOR DESIGN VARIABLES".

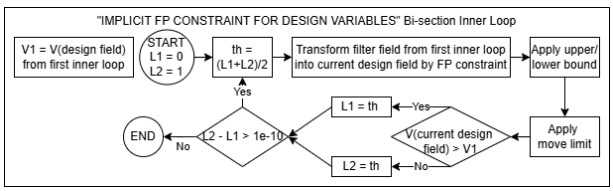

Fig. 4 Flowchart of the bisection inner loop for implicit FP constraint.

Since the expression of implicit filtering is the same as equation (14), the implicit FP constraint can be directly employed on the optimal design variables in the filter field ($\tilde{x}_e$) from the first bisection inner loop. The second bisection inner loop terminates when the volume of the design variables in the design field at the current iteration ($V_f(\bar{x}_e)_k$) equals to the volume of the optimal design variables in the design field from the first bisection inner loop ($V_f(\bar{x}_e)$). Then, the upper bound (=1) and lower bound (x_{min} = 10^{-6}) are employed. The move limit (δ = 0.2) is also employed to enforce that the value of element e in the design field at the current iteration ($\bar{x}_e)_k$ remains within the range [$(\bar{x}_e)_{k-1}$ - δ, $(\bar{x}_e)_{k-1}$ +δ].

The difference between β_1 in equation (17) and β in equation (22) is that β_1 is primarily used for eliminating intermediate elements generated by filtering process, while β is used to define the strictness of 0/1 constraints of the design variables in FP process. Thus, the equation β_1 = 1.2 β enforces β_1 > β relationship, meaning that the design variables in the physical field (from Heaviside projection) are closer to pure 0/1 design than the design variables in the design field (from Floating projection). Nevertheless, an excessively larger value of β_1 compared to β could lead to numerical instability. It is recommended to start with a small positive number like 10^{-6} to avoid numerical instability that occurs when a large value of β_1 excessively pushes the uncleared topology in the design field toward a 0/1 design.

The convergence criterion is divided into two parts: the smooth design criterion and the stopping criterion. The smooth design criterion is expressed as:

$$\max\left|(\bar{x}_e)_k - (\bar{x}_e)_{k-1}\right| \le 0.01 \quad (23)$$

Once the smooth design criterion is satisfied, pure image processing will be employed on design variables in the physical field to extract a pure 0/1 design. However, the extracted smooth design may not accurately represent a structural performance. Thus, a projection back to the original mesh is extracted to v_e. Then, a finite element analysis is conducted to calculate the structural compliance of a projection and stored as $C(v_e)$.

The stopping criterion can be calculated by:

$$\max(\tau_p, \tau_g) \le 0.01 \quad (24)$$

$$\tau_p = \left|\frac{C(\upsilon_e) - C(x_e)}{C(x_e)}\right| \quad (25)$$

$$\tau_g = \sum_e (\upsilon_e - x_e)^2 \Big/ \sum_e x_e \quad (26)$$

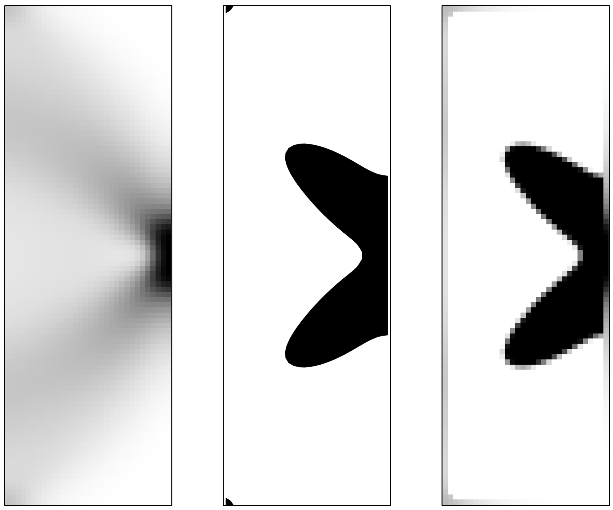

Fig. 5 (Left) A design variables in physical field, (Middle) A smooth design of a design variables, (Right) A projection of a smooth design.

From equation (24) to (26), τ_p is the relative difference between the structural compliance of a smooth design compared to the design variables in the physical field, τ_g is the geometry difference between a smooth design and the design variables in the physical field, $C(x_e)$ is the structural compliance of design variables in the physical field. If the stopping criterion is satisfied, the optimization can be stopped, indicating that the projection of a smooth design accurately represents the design variables in the physical field.

On the other hand, if the smooth design criterion is satisfied but the stopping criterion is not, this might be caused by too small value of β. Resulting in a large portion of intermediate elements in the design variables and the projection cannot accurately represent the current design variables in the physical field. Therefore, β should be further increased. The original FPTO recommends increasing β with $\Delta\beta$ = 1 every time the smooth design criterion is satisfied.

However, based on experimental numerical simulations of weight minimization, the optimization process tends to satisfy the smooth design criterion but not the stopping criterion. Thus, increasing β with $\Delta\beta$ = 1 every time the smooth design criterion is met might result in an excessive value of β , leading to instability when the optimization process is nearly complete. To address this, the value of β is calculated using a logarithmic function and can be expressed as:

$$\beta = a\log(iter) \quad \text{where } a > 0 \tag{27}$$

where $iter$ is the number of the current iteration and a is a constant that determines the steepness of the logarithmic function. In this setup, the value of β is equal to 10^{-6} until the first smooth design criterion is satisfied. Then, β is recalculated each time the smooth design criterion is triggered.

As the design variables approach the optimal solution, they become more sensitive to β. A slight increase in β can cause instability, preventing convergence. To mitigate this, a logarithmic function is used due to its characteristic rapid growth in the initial iterations, followed by a gradual slowdown over time, reducing the risk of instability. Fig. 6 shows the comparison of β values from the original function ($\Delta\beta$ = 1) and the logarithmic function. Each data point indicates the iteration where the smooth design criterion is triggered.

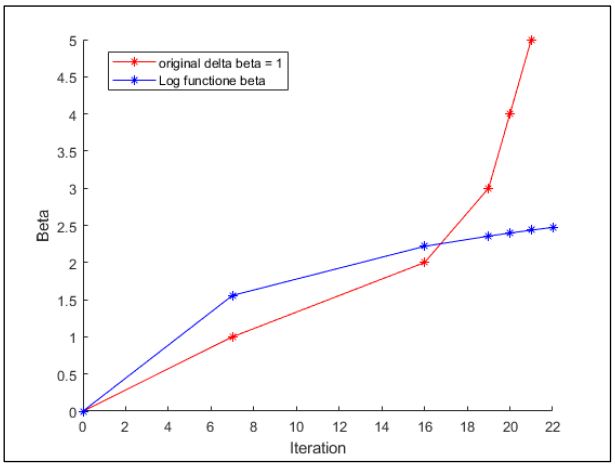

Fig. 6 Comparison of β values from the original and logarithmic functions.

3. Numerical example

The benchmark problem, the “two-bar truss” from [18], is used to demonstrate the potential of the proposed methodology. The details of the problem are shown in Fig. 7. The design domain is a rectangular block containing 32 elements in the x-direction and 96 elements in the y-direction, with the thickness of 1 unit. The fixed support is placed along the left end of the design domain, and a unit concentrated load is acting on the middle-end of the cantilever. The resulting optimal design resembles the shape of a two-bar truss and is shown in Fig. 8. The comparison of the results from the proposed methodology and the benchmark is shown in Table 1 and Fig. 9.

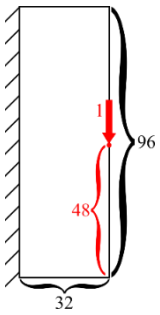

Fig. 7 Problem definition : two-bar truss [18].

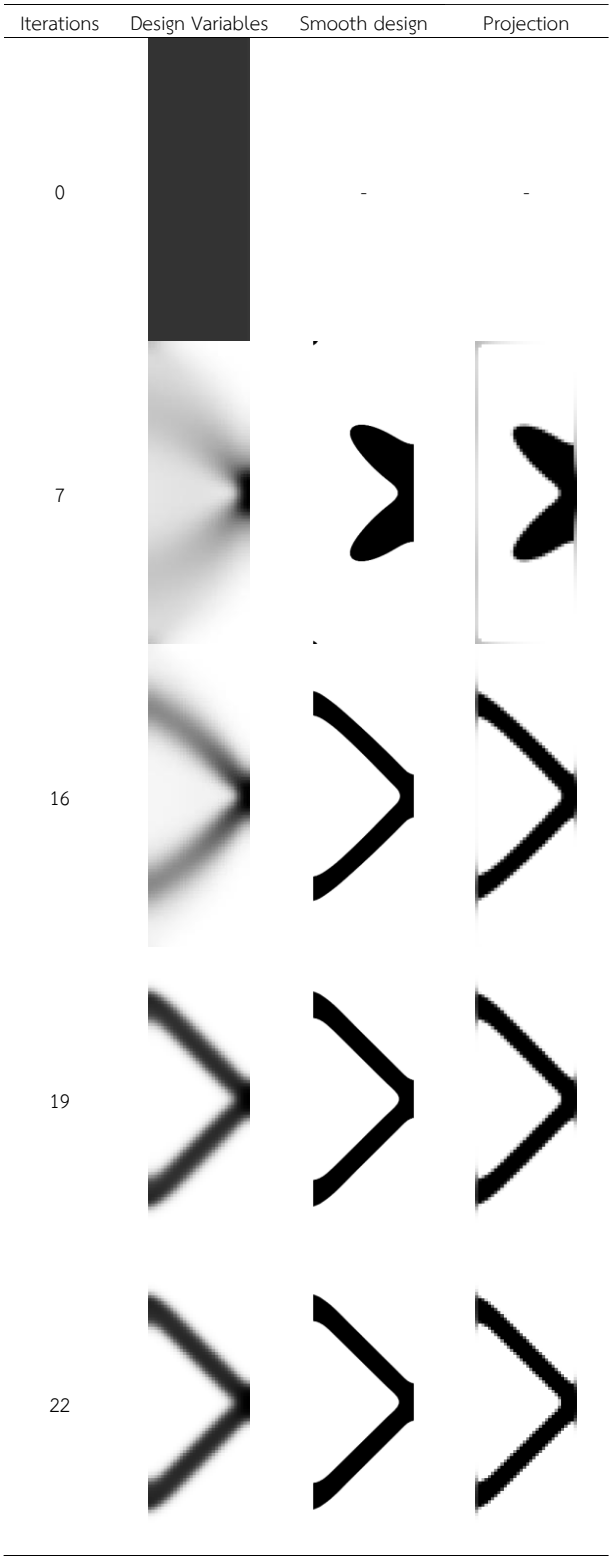

Fig. 8 Result images of the modified FPTO on "two-bar truss" problem.

Table 1 Performance metrics of the proposed methodology.

Method	Volume Fraction	Compliance Ratio	Number of elements	Computational Time
The proposed methodology	0.165	2.500	3072	97.50
Result from [18]	0.182	2.500	3072	25.00

*** Noted that the hardware specifications and underlying solvers used in [18] differ from those used in the proposed methodology, which can cause significant differences in computational time.*

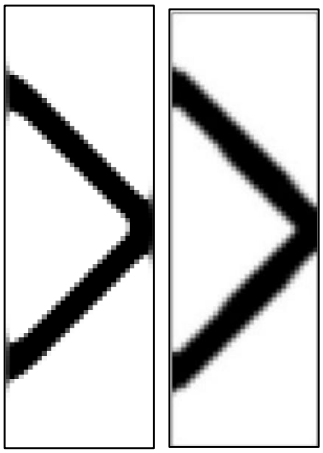

Fig. 9 (Left) An optimal design from the proposed methodology, (Right) An optimal design from [18].

4. Conclusions and Discussions

This paper presents a modified Implicit Three-field Floating Projection Topology Optimization (FPTO) method for weight minimization topology optimization. The proposed approach effectively reduces material usage while maintaining structural performance. Compared to the results from [18], the modified FPTO method achieves a lower volume fraction (0.165 vs. 0.182) while maintaining the same compliance ratio (2.500) and the same number of elements (3072). The computational time of the proposed method is significantly longer (97.50 vs. 25.00). It should be noted that differences in hardware specifications and underlying solvers between [18] and the proposed methodology could significantly affect computational time. This demonstrates the capability of the proposed method to produce lightweight and structurally efficient designs. Future work will extend this methodology to more complex structures, three-dimensional structures, incorporate multi-physics constraints, or explore manufacturability considerations to further enhance its practical applicability.

Acknowledgement

The authors would like to express sincere gratitude to Prof. Chongmin Song for his invaluable supervision, motivation, and provision of necessary resources to ensure the high quality of

this paper. Additionally, the author would like to gratefully acknowledge the Graduate School of Chulalongkorn University for the financial support of graduate studies, granted in celebration of His Majesty the King's 72nd Birthday Anniversary

References

[1] Su, R., Tangaramvong, S., and Huynh Van, T. (2023). An BESO Approach for Optimal Retrofit Design of Steel Rectangular-Hollow-Section Columns Supporting Crane Loads. *Buildings*, 13, pp. 328.

[2] Elelwi, M., Botez, R.M., and Dao, T.-M. (2021). Structural Sizing and Topology Optimization Based on Weight Minimization of a Variable Tapered Span-Morphing Wing for Aerodynamic Performance Improvements. *Biomimetics*, 6, pp. 55.

[3] Fritz, C., Fischer, L., Wund, E., and Zaeh, M.F. (2023). Inner design of artificial test bones for biomechanical investigations using topology optimization. *Progress in Additive Manufacturing*, 8, pp. 427-435.

[4] Sigmund, O. (2001). A 99 line topology optimization code written in Matlab. *Structural and Multidisciplinary Optimization*, 21, pp. 120-127.

[5] Wang, C., et al. (2021). A comprehensive review of educational articles on structural and multidisciplinary optimization. *Structural and Multidisciplinary Optimization*, 64, pp. 2827-2880.

[6] Bendsøe, M. (1989). Bendsoe, M.P.: Optimal Shape Design as a Material Distribution Problem. Structural Optimization 1, 193-202. *Structural Optimization*, 1, pp. 193-202.

[7] Xie, Y.M. and Steven, G.P. (1993). A simple evolutionary procedure for structural optimization. *Computers & Structures*, 49, pp. 885-896.

[8] Su, R., Boonlertnirun, P., Tangaramvong, S., and Song, C. (2024). Isosurface-based marching cube algorithm for smooth geometric topology optimization within adaptive octree SBFE approach. *Engineering Analysis with Boundary Elements*, 168, pp. 105920.

[9] Su, R., Tangaramvong, S., and Song, C. (2024). Automatic Image-Based SBFE-BESO Approach for Topology Structural Optimization. *International Journal of Mechanical Sciences*, 263, pp. 108773.

[10] Su, R., Zhang, X., Tangaramvong, S., and Song, C. (2024). Adaptive scaled boundary finite element method for two/three-dimensional structural topology optimization based on dynamic responses. *Computer Methods in Applied Mechanics and Engineering*, 425, pp. 116966.

[11] Huang, X. (2022) A Matlab code of topology optimization by imposing the implicit floating projection constraint.

[12] Huang, X. and Li, W. (2022). Three-field floating projection topology optimization of continuum structures. *Computer Methods in Applied Mechanics and Engineering*, 399, pp. 115444.

[13] Huang, X. and Li, W. (2021). A new multi-material topology optimization algorithm and selection of candidate materials. *Computer Methods in Applied Mechanics and Engineering*, 386, pp. 114114.

[14] Su, R. (2022). Automatic image-based SBFE approach for multiphase-materials topology optimization under dynamic loading. Ph.D. Dissertation, Chulalongkorn University, Thailand.

[15] Hu, J., Yao, S., and Huang, X. (2022). Topological design of sandwich structures filling with poroelastic materials for sound insulation. *Finite Elements in Analysis and Design*, 199, pp. 103650.

[16] Chen, W. and Huang, X. (2019). Topological design of 3D chiral metamaterials based on couple-stress homogenization. *Journal of the Mechanics and Physics of Solids*, 131, pp.

[17] Rozvany, G.I.N. (1989) Structural Design via Optimality Criteria: The Prager Approach to Structural Optimization. Kluwer Academic Publishers.

[18] Bruggi, M. and Duysinx, P. (2012). Topology optimization for minimum weight with compliance and stress constraints. *Structural and Multidisciplinary Optimization*, 46, pp. 369-384.